NASA TECHNICAL MEMORANDUM

NASA TM-75874

HIGHLY SEPARATED TRANSONIC FLOWS

A. Farcy, V. Mercier, R. LeBlanc, R. Goethals

Translation of "Ecoulements Transsoniques Fortement Decolles", Association Aeronautique et Astronautique de France. Colloque d'Aerodynamique Appliquee, 16th, Lille, France, Nov. 13-15, 1979. paper NT 80-18, 20p. (A80-36849).

NATIONAL AERONAUTICS AND SPACE ADMINISTRATION
WASHINGTON, D. C. 20546 MAY 1981

STANDARD TITLE PAGE

1. Report No. NASA TM-75874	2. Government Accession No.	3. Recipient's Catalog No.
4. Title and Subtitle: HIGHLY SEPARATED TRANSONIC FLOWS		5. Report Date MAY 1981
		6. Performing Organization Code
7. Author(s): A. Farcy, V. Mercier, R. LeBlanc and R. Goethals		8. Performing Organization Report No.
		10. Work Unit No.
9. Performing Organization Name and Address: SCITRAN, Box 5456, Santa Barbara, CA 93108		11. Contract or Grant No. NASw-3198
		13. Type of Report and Period Covered: Translation
12. Sponsoring Agency Name and Address: National Aeronautics and Space Administration, Washington, D.C. 20546		14. Sponsoring Agency Code

15. Supplementary Notes

Translation of "Ecoulements Transsoniques Fortement Decolles" Association Aeronautique et Astronautique de France. Colloque d'Aerodynamique Appliquee, 16th, Lille, France, Nov. 13-15, 1979. paper NT 80-18, 20p. (A80-36849).

16. Abstract

The first experimental results on highly separated transonic flow is reported, using as a model a rectangular tube placed at strong incidence (up to 40°) in a transonic jet. Attention is given to the wind tunnel, to photographic visualization of the flow, and to measurements by pressure probes, hot-wire anemometry and laser anemometry. The simultaneous use of different means of measurement has provided a good description of the phenomenon, and has indicated the existence of shocks and their stability, as well as the existence of the bubble, its dimensions, and in particular, the reattachment of its front. The results show that the bursting (or transition) of the bubble front is produced at an unstable position and creates a point of turbulent intensity which diffuses over the entire height of the flow.

17. Key Words (Selected by Author(s))	18. Distribution Statement: Unclassified - Unlimited		
19. Security Classif. (of this report): Unclassified	20. Security Classif. (of this page): Unclassified	21. No. of Pages: 26	22. Price

HIGHLY SEPARATED TRANSONIC FLOWS*

***/1

A. Farcy, V. Mercier, R. LeBlanc, R. Goethals**

1. INTRODUCTION

This report describes the first experimental results obtained for highly separated transonic flow. The model is a nozzle having a cross-section placed at a high incidence angle (up to 40°) in a transonic jet. A separation bubble appears along the lower leading edge (Figure 1). The resulting flow is very perturbed and difficult to predict theoretically. If the model represents an aircraft motor air inlet, one can then appreciate operational difficulties for the motor under such conditions. The purpose of this work is to test experimental methods which are capable of providing reliable results.

The definition of the most interesting configuration, which was the object of a preliminary study [1] is briefly described in Chapter 2. The investigation procedures of the flow are described and discussed in the following chapters. We are dealing with visualization and measurements with laser and hot wire anemometers. We will see that the combination of these means in the future will lead to a detailed knowledge of this type of flow.

2. WIND TUNNEL AND MODEL--SELECTION OF THE CONFIGURATION

2.1. Wind tunnel and model

*Research carried out with the contribution of the DRET Contract no. 79/069. November, 1979.
**CEAT-ENSMA - Poitier.
***Numbers in margin indicate pagination of foreign text.

The transonic jet, the model and its support are shown in Figure 2. The air is supplied by a HP (high pressure) network (200 bars) from CEAT, expanded to 4 bars maximum in a $4m^3$ container which contains a heat exchanger. The settling chamber is a 0.125 m^3 caisson attached to the chamber. The transonic nozzle with a cylindrical wall with dimensions of 100x 40 mm^2 cross-section is attached to the caisson. The high contraction ratio (34) assures a uniform jet and fine frontal layers which, together with filter screens mounted between the chamber and the caisson, will only bring about a small degree of turbulence in the free jet on the order of 1%. The measurement of the stagnation conditions p_t and T_t is performed in the chamber as well as the sensing of the flow using the laser and anemometer. For the tests described here the inclination of the jet with respect to the horizontal is 40°.

The model has a high H equal to 40mm and has a chord of 80mm. It is made up of two plates 250mm long, with sharp leading edges. The lateral walls go beyond the plates by 20mm and its edges are sharp in order to form guard plates. The windows have an optical quality and allow flow visualizations and laser anemometry. They are recessed into the lateral walls. They are installed on hinges and can be easily opened in order to allow easy cleaning of the windows, required for laser anemometry.

A diffuser with a total angle of 7° is installed at the outlet of the model. It is followed by a deformative throat, consisting of a spring loaded steel sheet, which allows adjustment of the flow rate.

The entire complex is installed on a support which can be varied in incidence angle (from 0 to440°), which allows one to carry out the tests described below.

2.2. Selection of the configuration

The preliminary tests on the functioning of a model of an air inlet have shown that a large separation bubble exists for an incidence angle equal to 40°, but it is very much reduced for α = 20° (Figure 4). The variation of the flow rate coefficient σ seems to have a small effect on the geometry of the bubble. On the other hand, we have shown that the average Mach number measured in a section x = 4H, for example, can vary greatly with σ. We have concluded that the interesting configuration for systematic measurements of velocity and turbulence intensity using laser anemometry which is the main objective of Reference 1, was obtained at 40° with a throat opening equal to 14mm.

A map σ(M) was drawn for the section x = 8H of the model in the present study. σ and M are derived from measurements of two stagnation pressures at z = 5 and 15mm and the wall pressure, where the flow in this section was sufficiently homogeneous. The Mach number of the free jet is 0.7. The results are shown in Figure 3. The flow rate coefficient σ increases when the height of the throat h increases and the incidence angle α decreases. The average Mach number in the section follows the same trend for h = 16 and 20, but there is an inversion which occurs for h = 12 and 8 when α = 30°. Since we do not have a rigorous explanation, we will make two remarks: (1) For these two values of opening, the throat is very close to sonic conditions (M^* = 1) if we consider the value of the average Mach number at x = 8H (Figure 3). (2) The substantial development of the bubble at 40° results in a homogeneity at 8H which is less good than for α = 20° and three pressure measurements are not sufficient for obtaining a good accuracy.

The configuration retained for the comparative study of the test means was α = 40°, h = 14mm, which is an operating point estimated so that $\sigma \simeq 0.57$ and $M \simeq 0.39$. These characteristics are close to those imposed under contract. They result in a highly separated flow with a transonic region and shock waves,

as the flow visualizations described in the following chapter will show.

3. VISUALIZATIONS OF THE FLOW*

3.1. Test equipment

The installation is equipped with a strio-ombroscopy table produced at CEAT and which has two mirrors with a diameter of 300, F = 3m. The image is formed on the sensitive plate of a photographic chamber or on the film of a rapid camera.

The photographs on 9x12 plates with a sensitivity equal to 400 ASA are made using two types of luminous sources: Either a continuous mercury vapor lamp, and the exposure time has been 1/500 or 1/250 seconds, or a spark, with a duration close to 1 μs. /3

The films of the 25 images with the format 15x24 were made with a camera of the LCA of type CI4 at frequencies between 8×10^4 to 10^6 frames per second. The image from the optical system is passed to a rotating mirror and then to an objective battery which then forms the definite images on the film. The useful sweep angle is 72°; the velocity of the turbine provides the rotation of the mirror which is controlled electronically. The beginning of the illumination must be synchronized with the position of the mirror so that the 25 images are formed once only. The automatic triggering of the aluminum source and measurement of the velocity of the mirror are accurate to 1/1000. The quality factor, that is, the ratio of the time interval between two images and the exposure time,is 3.1. At 10^6 images per second, the turbine rotates at 4000 rps and the exposure time of one image is 314 ns. We use 35 millimeter film with a

*With the participation of Mr. Antigny, photographer.

sensitivity of 400 ASA, sometimes pushed to 3000 ASA during development. The luminous sources are of two types, depending on the frequencies at which the frames are made: Either a flash generator for 100 μs (10^6 images per second) or a bursting tube whose flash time is adjustable.

Let us mention the recording on a magnetoscope of the strio-ombroscopic image, when a parametric study is made for example, in order to avoid an observation test repetition. One interesting application is to find the unsteady regime such as the pulsation of the bubble. The mediocre quality of the reconstituted image does not allow a quantitative evaluation. Let us also mention that the wall visualizations, realized afterwards on an oil film and black smoke, did not produce any significant three-dimensional effects.

3.2. Photographs on plates

Examples of photographs on plates of ombro and strioscopy using flashes are shown in Figure 4a. They were taken during systematic flow visualization tests with an open throat, open to a maximum (h = 20mm). The strio and ombroscopic techniques respectively show the gradients and the variations of the density gradients of the flow and are, therefore, complementary.

The main interest in the plate photographs is the good quality of the image which results from the dimensions and the sensitivity of the support. The impressions of a richness of information given by this technique must be materialized by the analysis and the exact description of the events. Below we will attempt to discuss the results and will not attempt to give definite information about the aerodynamic phenomena.

The separation bubble $\alpha = 40°$ is characterized by two methods in the forward part. Its boundary, which is a highly sheared layer, is characterized by a change in color (gray/black)

in strioscopy, and by a dark/white line in ombroscopy. The gradients are practically constant in the highly accelerated region above the bulb, and this brings about a uniform dark zone in strioscopy, just like the "wake" of the bubble. This wake is caused by the bursting of the shear layer, the boundary of the bubble. This transition is very rapid as the two ombroscopies clearly show. It is produced at the average position $x \leqslant H/2$. The wake diffuses in the upper direction and downwards. These boundaries are very highly shredded, and show large /4 structures which extend over the entire height after $x \simeq 3H$. After mentioning the "large structures" emitted by the bubble, it is appropriate to speak of "small structures" which make them up and which are visible on the ombroscopies. Therefore, we can see the net requirement for having quantitative information using sensors.

Therefore, we can draw practical information by analyzing several samples of the same flow, and during its evolution over time (statistical aspect). The normal shocks which delimit the supersonic region in the upper forward part of the model vary in position. The transition of the upper boundary varies also as well as the boundary structures of the bubble and its wake. It is difficult to go further in the interpretation and we, therefore, again see the requirement for continuous recording of the phenomena.

3.3. High speed films for viewing

Several rapid films were made, strio and ombroscopic, at 75,000, 100,000, 250,000 and 1,000,000 images per second. Figure 4b shows 10 successive years of a strioscopy filmed at 250,000 images per second. The enlargement of the zone of interest is important and the quality is poorer than with plates. One can, nevertheless, observe certain characteristic evolutions. For example, in photograph 1, above the hot wire probe, we see an

egglike structure with a central core. This appears clearly in photograph 4 and disappears in photograph 8. Therefore, it exists for around 20 μs. This evolution is relatively slow as well as the evolution of the normal shocks which remain practically stable for the entire series. From this we can conclude that the fluctuation frequency of an average boundary over which there are shocks is less than 20 kHz. Also, we should note that the inclination of the structure is also visible on the plate photographs which shows their coherence and their deformation due to the high veolocities of the upper layers. Photographs at smaller speeds and quantitative measurements are necessary here.

During preliminary tests, we also filmed a strioscopy at 8000 images per second with a HICAM camera having a rotating prism. The Mach number at the inlet was higher: 0.85 to 0.71 for the configuration adapted after that. The flow remains supersonic over a larger distance, which is not important for our work, which has to do with the investigation of a technique. This film essentially shows that the average bubble boundary is stable up to 4 kHz*, that the transition point (also so that $x \leq H/2$) is displaced by a few millimeters along the average stable line, that the normal shocks are unstable and that their fluctuations seem to be tied to those of the transition point.

Finally, we should remark that if the existence of the bubble raises no doubt about the photographs, the reattached position cannot be estimated with accuracy. /5

3.4. Exploitation of the photographs using equidensity techniques

The photographs presented in the previous paragraphs were analyzed using the equidensity technique. An example of this

*That is, within the limits of the utilization of the camera.

is given in Figure 5. This is a sequence of a few successive images of a rapids filmed at 100,000 images per second. The exposure time is 3.14 μs. The technique used consists of translating the various densities of a black and white original by various colors. For this we make several copies of the original on a special film (Agfacontour) which behaves both as a positive and a negative at the same time, and which gives an image of a single density level to the original. The width of the region depends on the color temperature of the light utilized for exposure; its position in the gray levels is determined by the exposure time. It is then sufficient to take equidensity prints obtained on a colored film with a different filtering in order to obtain the final results.

This procedure makes the strioscopic plates more readable by giving a fine description of the details in the zones with a high gradient (boundary of the bubble). We are, therefore, free from chromatic abberations and problems of luminous sources which are related to color strioscopy with a dispersion prism.

The 10 images of Figure 5 cover a time interval of 100 μs. As in Figure 4b, the large convection structures in the flow appear clearly as well as their inclinations and their rapid deformation. Examination of the bubble boundary of separation shows that it has oscillations after $x = H/2$, particularly visible on images 5 and the following. These oscillations are amplified and are accompanied by phenomena of particle entrainment of the fluid by the accelerated layers. A complete cycle seems to be produced at 7 to 10 images which corresponds to frequencies of 10 and 15 kHz, the order of magnitude found using spectral analysis (see Chapter 5).

For the sections $x > 4H$, the gradients become smaller, the strioscopic plates do not give much information.

4. MEASUREMENTS USING LASER ANEMOMETRY [1]

4.1. Apparatus

The laser anemometry chain developed by the CEAT by ARDONCEAU for supersonic flow applications [2] allowed us to obtained particularly interesting results on the shock-boundary layer interaction [3] and for the air inlets which we are discussing here [1,4].

Figure 6a gives a view of the laser anemometer on a carriage in front of the installation. A 5 W coherent radiation laser provides a 2 W bundle at the light 5145 A. The laser unit-optical head (bundle divider and Bragg cell) is displaced along a carriage commanded by the IBM 1800 computer. The Bragg (TSI) cell excited at 40 MHz gives fringes and the velocity direction is derived from the frequency of the resulting signal: /6

$f_D > 40$ MHz velocity opposite to the direction of the fringes,

$f_D < 40$ MHz velocity in the direction of the fringes

The interfringe utilized here is between 10 and 15 μ and the diameter of the section of the test volume varies between 0.3 and 0.6 mm depending on the focal length of the condensor placed after the bundle divider. The light diffused by the particles (seeding with dioctyl phthalate with diameters of 0.7 to 1.3 μ) is captured with direct diffusion by a lens having a very wide opening (diameter 60mm, F = 90mm) and is focused on the diaphragm of a photomultiplier (RTC, XP 1110).

The signals coming from the photomultiplier are treated by counting using a digital counter studied at the CEAT and developed together with DELTALAB (DELTALAB - CEAT ANL 200). The frequency range which can be measured extends from 10 kHz

to 50 MHz, which allows measurement of velocities of a few cm/sec to more than 500 m/sec, depending on the characteristics of the optical equipment. The resolution is 5 ns. The high amplitude signals are eliminated and the numerical validation (which only records particles which pass in the plane of the fringes and perpendicular to it) is done with double counting with 5 and 8 alternations. The outputs are numerical (2*16 bits for nonvalidated measurements and 12 bits for validated measurements) as well as analog (rapid 12 bit converter). A timing allows a rapid rate (800,000 points per second at 50 MHz) or a slow rate (800 pts/sec) for the acquisition with telephone cable on a IBM 1800 computer. Since the measurement rate does not affect the arrival of particles, it was not necessary to carry out a correction due to a possible bias due to sampling (over estimation of high velocities).

The averages and standard deviations of the frequency are calculated a first time for several erroneous values, which could exist at frequencies which are very far away from the maximum of the histogram, and this is eliminated with the test $f(I) \quad [f \pm 3\sqrt{f'^2}]$.

4.2. Measurement of longitudinal velocities and their fluctuations

The average longitudinal velocities $\bar{u}$ and the mean quadratic value of their fluctuations u' are shown in Figure 7a. The position of 5 planes of measurement is indicated on the diagram. The soundings were made every 2 mm and sometimes every 1 mm (bubble) at the height H. Below we will summarize what can presently be derived from applied laser anemometry, applied to a transonic flow which is highly separated and violently perturbed.

The bubble is obviously present. It consists of a region of small velocity, 0 velocity, and a return velocity region with

8 mm for H, limited by a thin layer of 4 mm which is very highly accelerated. The return velocities are maximum at 2 H where they exceed 50 m/s. The reattachment is produced between 3 and 4 H. The measurements were repeated in the bubble (x = H/2) successfully.

We measured maximum velocities of 280 m/s (at H/4 and H). Considering the sizeable fluctuations (up to 40 m/s at H for z = 12 mm) we can explain the existence of the transonic region and the shocks observed in the photographs. The instability of of the shocks will be the result of this fluctuating combination, probably also related to that of the transition point.

Substantial fluctuations observed in the center of the profiles u' for x = H/4, H/2, H and which then diffuse over the entire height, could come from the strong shear demonstrated before, but also it could be caused by the possible instability of the boundary. In the following paragraph, we will show how this hypothesis has to be rejected. Outside of this maximum, the turbulence is practically constant and its value is two to three times greater in the bubble than in the upper part, and this is true up to x = 2H. The diffusion in the entire field is broken up for x = 4H and is complete at x = 8H, where the average speed $\bar{u}$ is practically homogeneous.

Without entering into a detailed analysis of the flow, we can see that the turbulence referred to an average speed of 100 m/s goes from 10 to 40% from the inlet to the outlet. This is a substantial increase.

4.3. Measurements of transverse velocities and of their fluctuations

The transverse velocities for x = 0, H/4 and H/2 are large and confirm the existence of the bubble. The inclination of the

streamlines downwards which leads to reattachment is substantial at 2 H and almost disappears at 3 H. Reattachment between 3 and 4 H is, therefore, mostly indicated by the disappearance of the longitudinal return speeds than by the inclination of the streamlines. The high turbulence, that is, u' as well as v', explains this behavior.

The large vertical velocity gradient at x = H/4, y = 6,8, results in a rather weak increase in v' at H/2 which disappears rapidly. There is no substantial increase in the vertical fluctuations at the bubble boundary, which would not be the case if it were oscillating. This important remark confirms, therefore, the hypothesis made in the preceding paragraph, that only the shear of the viscous boundary layer which must explode between 0 and H/4 (Figure 7a) is responsible for this turbulence increase.

The intensity of the vertical fluctuation at the output related to 100 m/s is less than 20% . It is one-half of the longitudinal value, but v'_{moy} (average) is very close to u'_{moy} at the inlet.

5. MEASUREMENTS USING HOT WIRE ANEMOMETRY /8

5.1. Problems related to compressibility

The voltage fluctuations at the terminals of a hot wire maintained at a constant temperature and subjected to a compressible flow depend on velocity fluctuations, the specific mass and the total temperature of the gas. Generally, it is assumed that the sensitivity coefficients at the speeds and specific masses are equal for a Mach number of $M \geq 1,2$ [5]. It is then possible for supersonic flow, to reduce the number of parameters contributing to the wire response to two (mass flow rate ρu and total temperature T_t) and to use various separation procedures

The spectrum analyser used is the SAICOR 51A type which produces spectra on 200 points transferred numerically to a data acquisition center IBM 1800.

In order to proceed with the statistical analysis of the hot wire signals, the recorded signals are reread at a tape rate of 7.5 inches per second (19 cm/sec) and then sampled by the IBM 1800 at a frequency of 8.4 kHz. This procedure allows the simulation of a rapid acquistion at 135 kHz.

5.3. Spectral analysis

Figures 8a and 8b show the examples of spectra (spectral energy density) at two sections $x = H$ and $x = 4H$ of the air inlet. The hot wire is oriented perpendicular to the flow plane. For the section $x = H$ we avoided the zone where there is a strong recirculation ($z < 5$ mm) and the zone where the Mach number is greater than 0.8 ($z > 14$ mm).

If we take into account the fact that we do not have access to the global level of energy and that we cannot position the spectra with respect to one another, we can recognize that the exploitation of the spectra in this form is difficult. We would remark that the spectra of Figure 8b for $z \gtrsim 12$ mm have a characteristic peak at 38.5 kHz, probably due to a vibration of the wire due to a stress effect. In order to avoid this drawback, we are considering using modified probes with shorter posts.

Figure 8c shows the variation of the region of frequency which contains the maximum energy in the sections $x = H$ and $x = 4H$. The hatched area corresponds to an estimation of the narrowest frequency band which contains 50% of the total energy. The examination of this figure leads to the following remarks:

for example, the method of fluctuation diagrams.

In general, the transonic case does not allow this simplification and is complicated due to the existence of shocks which are often unstable at the level of the probes. This then directed our work towards hot wire measurements. We concentrated on two points which were more qualitative than quantitative. The purpose was to obtain additional information on the global behavior of the flow instead of precisely describing the kinematic field (see Chapter 4).

The tests were performed by making the following precautions:

- limitation of the total temperature fluctuations by controlling the temperature gradients. The generating temperature is maintained by reheating (see Chapter 1) at the level of ambient temperature,
- functioning of the wire with strong overheating (0.8),
- if possible, measurements in zones where the Mach number is too close to 1 are avoided.

5.2. Apparatus

The hot wire probes are DISA 55 A 53 subminiature probes with long posts (3mm) mounted in a cross-configuration within a folded monel tube with an external diameter 2mm. The anemometers used are the DISA 55 M type, having the standard CTA 55 M 10 ridges. The passband of the complex is substantially above 100 kHz.

The opposite signals of the anemometers are centered and then recorded on an FM Bell & Howell RD-378/U magnetic recorder. The tape speed rate is 100 inches per second (3.04 m/s) for recording which assures a passband of 500 kHz for a signal to noise ratio of nominally 32 dB.

a/ the average width of the most energetic band varies from 1/2 decades for x = H to 2/3 decades for x = 4H which indicates an energy transfer towards the smaller turbulent scale.

b/ in the zone of the section x = H where the fluctuations are more intense (z ≃ 10 mm), the energy maximum is centered at the frequency f* ≃ 15 kHz, which corresponds to large structures of high energy having the size:

$$\Lambda = \frac{\bar{u}}{f^*} = \frac{155 \text{ m/sec}}{15\ 10^3/\text{sec}} \simeq 10 \text{ mm} \quad \text{or } H/2$$

c/ in the section x = 4H we see a substantial reduction in the highest energy frequencies in the zone of the border wake of the separation bubble (z ≃ 8 to 16 mm). The characteristic scale estimated previously varies from:

$$\Lambda = \frac{\bar{u}}{f^*} = \frac{70}{25.10^3} \simeq 2{,}8 \text{ mm} \quad \text{or } H/8$$

in the lower quarter of the section to:

$$\Lambda = \frac{130}{8.10^3} \simeq 16 \text{ mm} \quad \text{or } 3H/4$$

in this wake zone whose thickness is on the order of H/2.

Therefore, we can assume that these large convection structures, transported by the flow, are deformed and inclined by the vertical velocity gradient, which appears clearly on the various flow realizations (Figures 4 and 5). /10

6. DISCUSSION OF RESULTS-FUTURE DEVELOPMENTS

The combination of the techniques of qualitative measurements and quantitative measurements is necessary for the analysis of complex flows such as occur in a transonic air inlet

with a large incidence angle. A single method used within its limits could not give the information obtained from several additional methods, even though they were only partially exploited. Here we present a synthesis of the results which show how measurements made in highly separated transonic flows using flow visualization (V), filmed visualization (VF) measurements with pressure probes (P), laser anemometry (AL) and hot wire (FC) are all complementary.

The simultaneous use of V, VL, P and AL gives a good general description of the phenomena and its evolution as a function of the various parameters. By a general description, we mean the following: (1) the existence of shocks and their stability (V, VF); (2) existence of the bubble (V), its dimensions (V, AL) and in particular, the reattachment (AL) and the oscillation of the boundary (VF, AL); (3) the flow rate coefficient by an approximate but sufficient evaluation of the pressures (P).

The description of the turbulent nature of the flow is a tributary of the combination V, VL, AL and FC. The first results presented here show that the flow (or transition) of the bubble boundary occurs at an unstable position (V and VF) and creates a turbulence intensity point which diffuses over the entire height of the flow (AL, FC). We found large structures (V, FC) which rapidly evolve (VF, FC) and are inclined due to the effect of a velocity gradient (V, FC). The intensity of the fluctuations is uniform in the bubble, outside of it (outside of the shear layer) and far downstream (AL).

Finally, we estimate the evolution of scales of turbulent phenomena, especially large convective structures (VF, FC) and we propose an experimental series in order to characterize the distortions which they will produce in the flow (FC).

REFERENCES

(1) R. LeBlanc, Ph. Thiebault, P. Ardonceau, R. Goethals. Experimental study of transonic air inlets at large incidence angles, contract DRET no. 77/214, final report nov. 1978.

(2) P. Ardonceau. Application of laser anemometry to supersonic aerodynamics. Third Cycle Thesis, Poitiers, 1974.

(3) P. Ardonceau, T. Alziary de Roquefort, D. H. Lee and R. Goethals. "Turbulence behavior in a shock wave/boundary layer interaction" AGARD Conference on "Turbulent boundary layers - Experiments, Theory and Modeling", The Hague, Sept. 24-26, 1979.

(4) Ph. Thiebaut, P. Ardonceau, R. LeBlanc and R. Goethals. "First measurements in highly separated transonic flow" Mechanics Research Communications, vol. 6(2) pp. 113-114, 1979.

(5) M. V. Mokovin. "Fluctuations and hot-wire anemometry in compressible flow" AGARDograph no. 24, Nov. 1956.

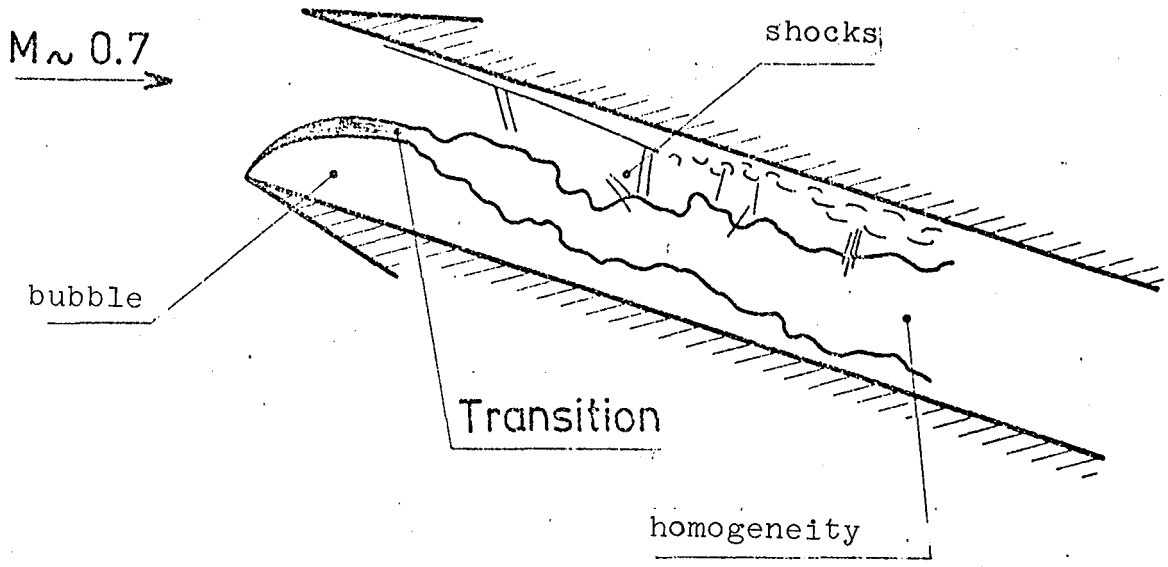

FIGURE 1. EXAMPLE OF TRANSONIC FLOW WHICH IS HIGHLY SEPARATED

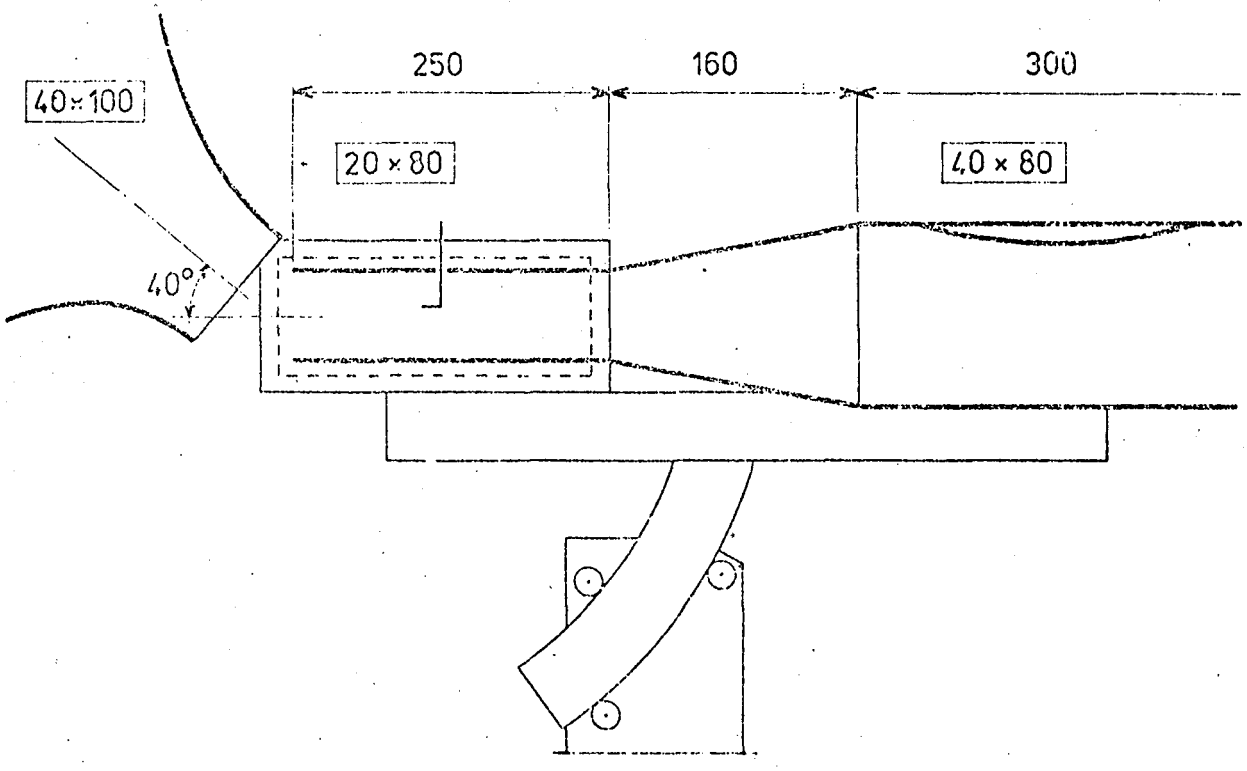

FIGURE 2. DIAGRAM OF INSTALLATION

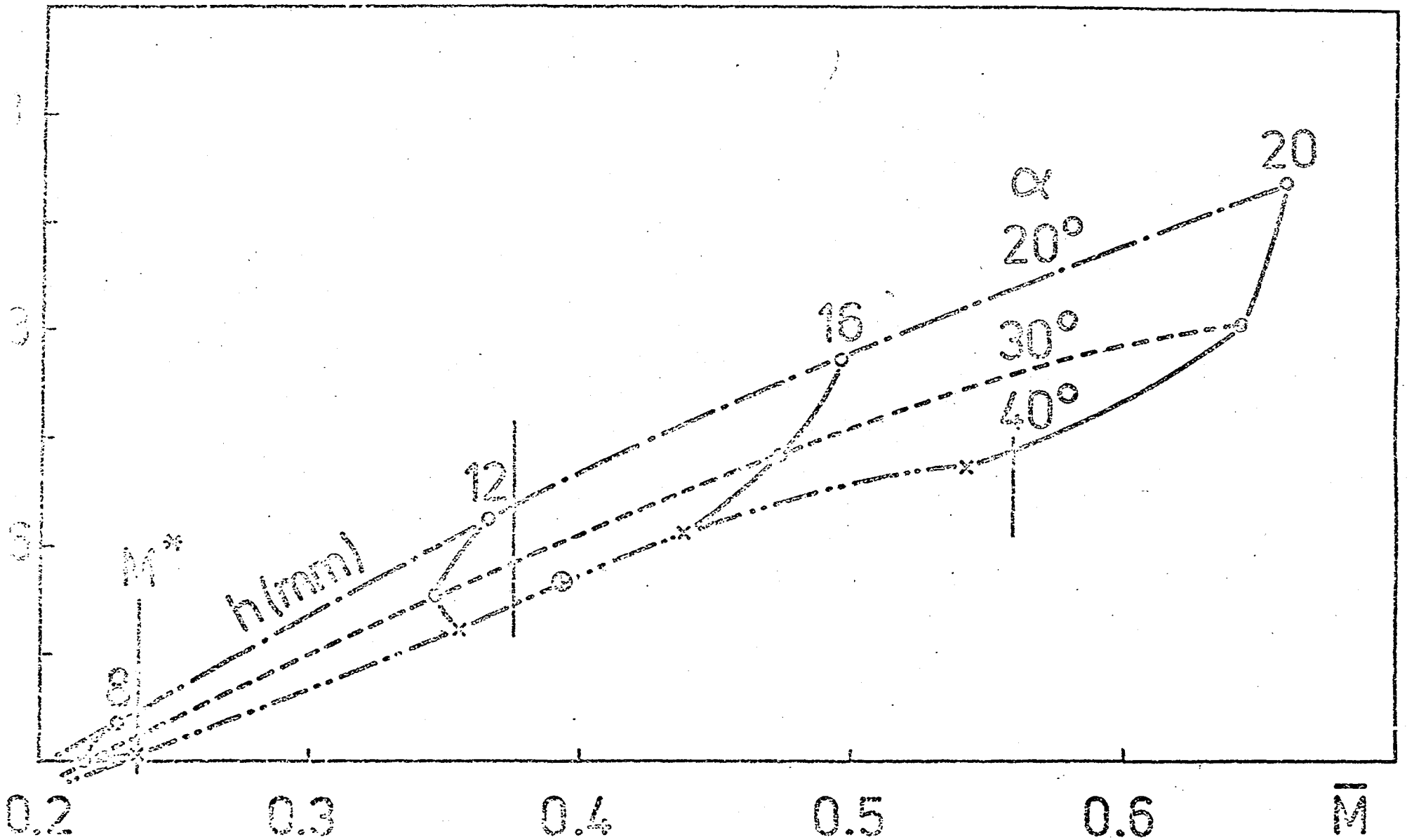

FIGURE 3. FLOW RATE COEFFICIENT

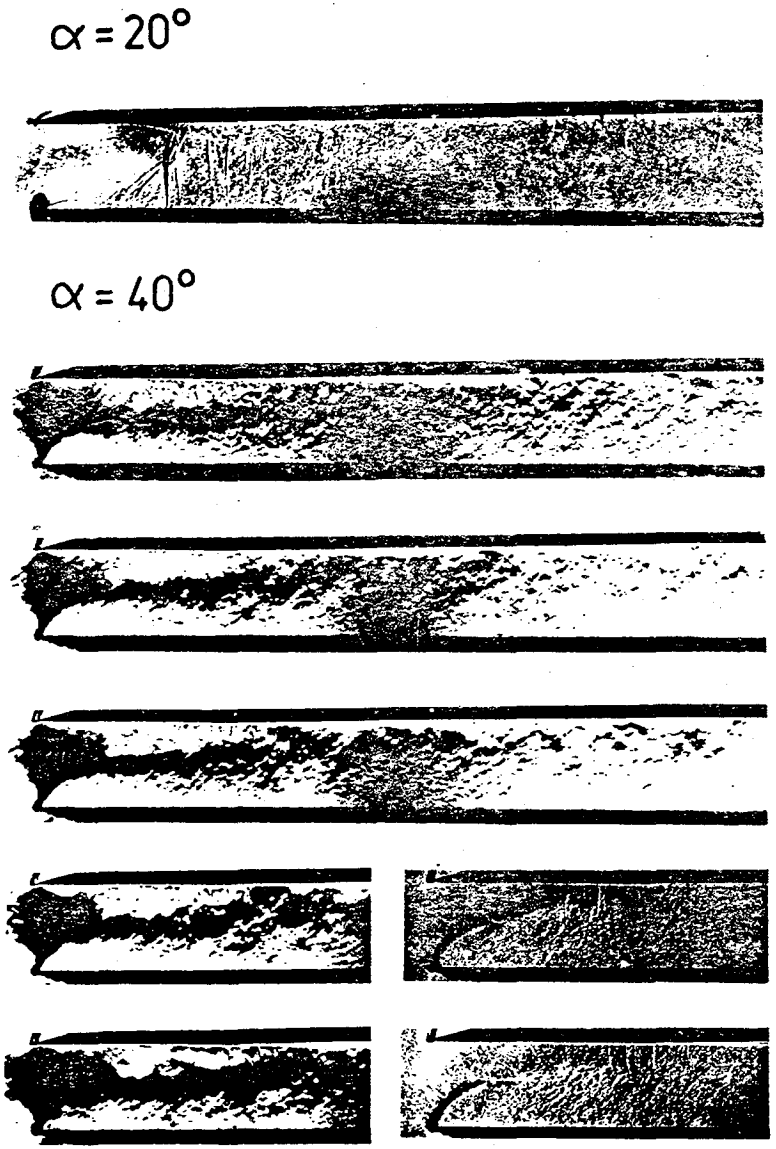

a)_ plate 9×12 _ t≃1 μs

b)_ Film 250000 im/s

t=1.25 μs Δt= 3.88 μ

FIGURE 4. FLOW VISUALIZATIONS

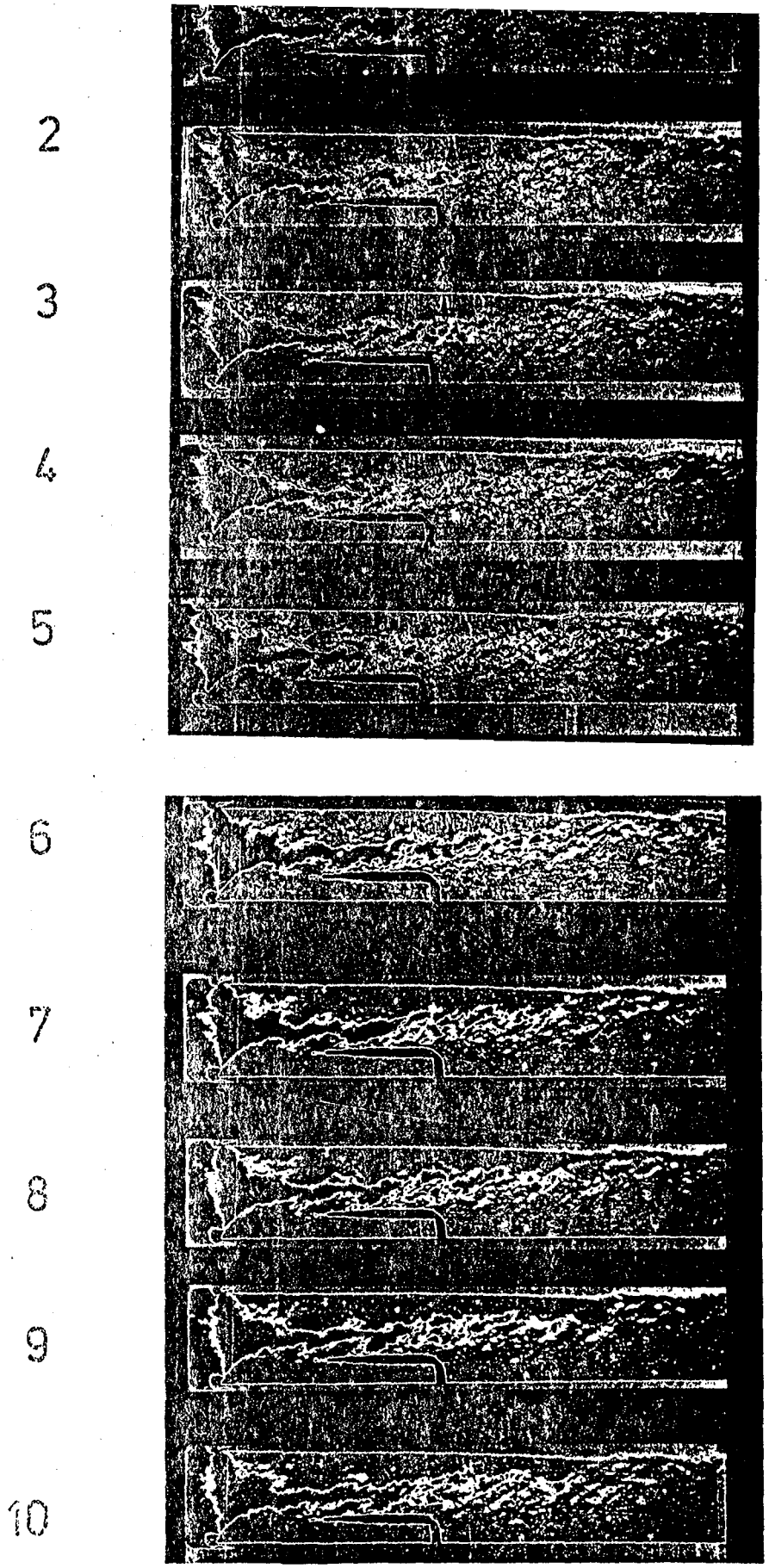

FIGURE 5. EQUIDENSITY OF STRIOSCOPIC FILMS

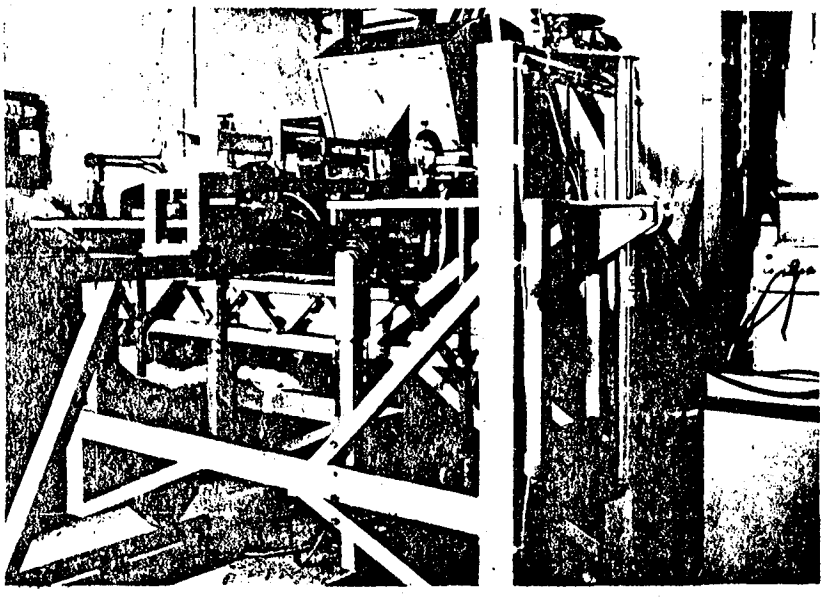

a) Model wind tunnel and laser anemometry

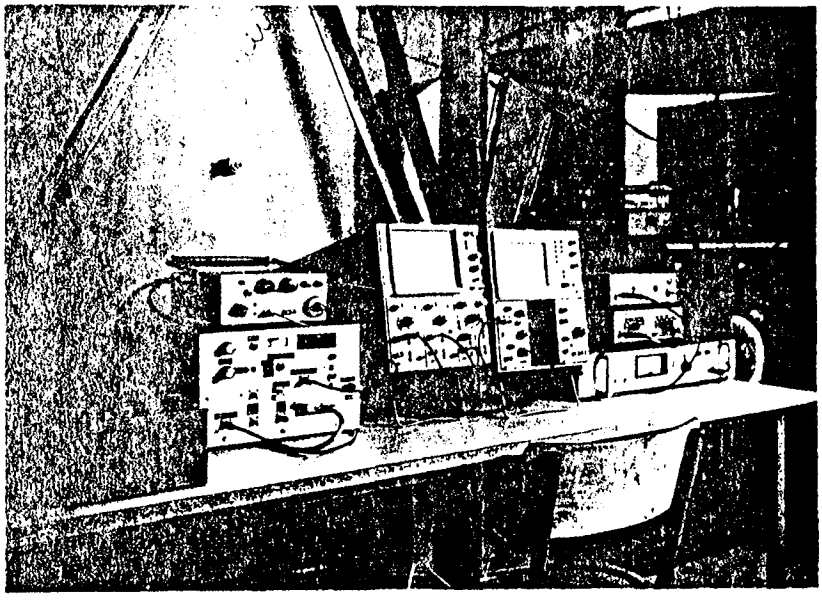

b) Processing electronic

FIGURE 6. INSTALLATION AND LASER ANEMOMETRY

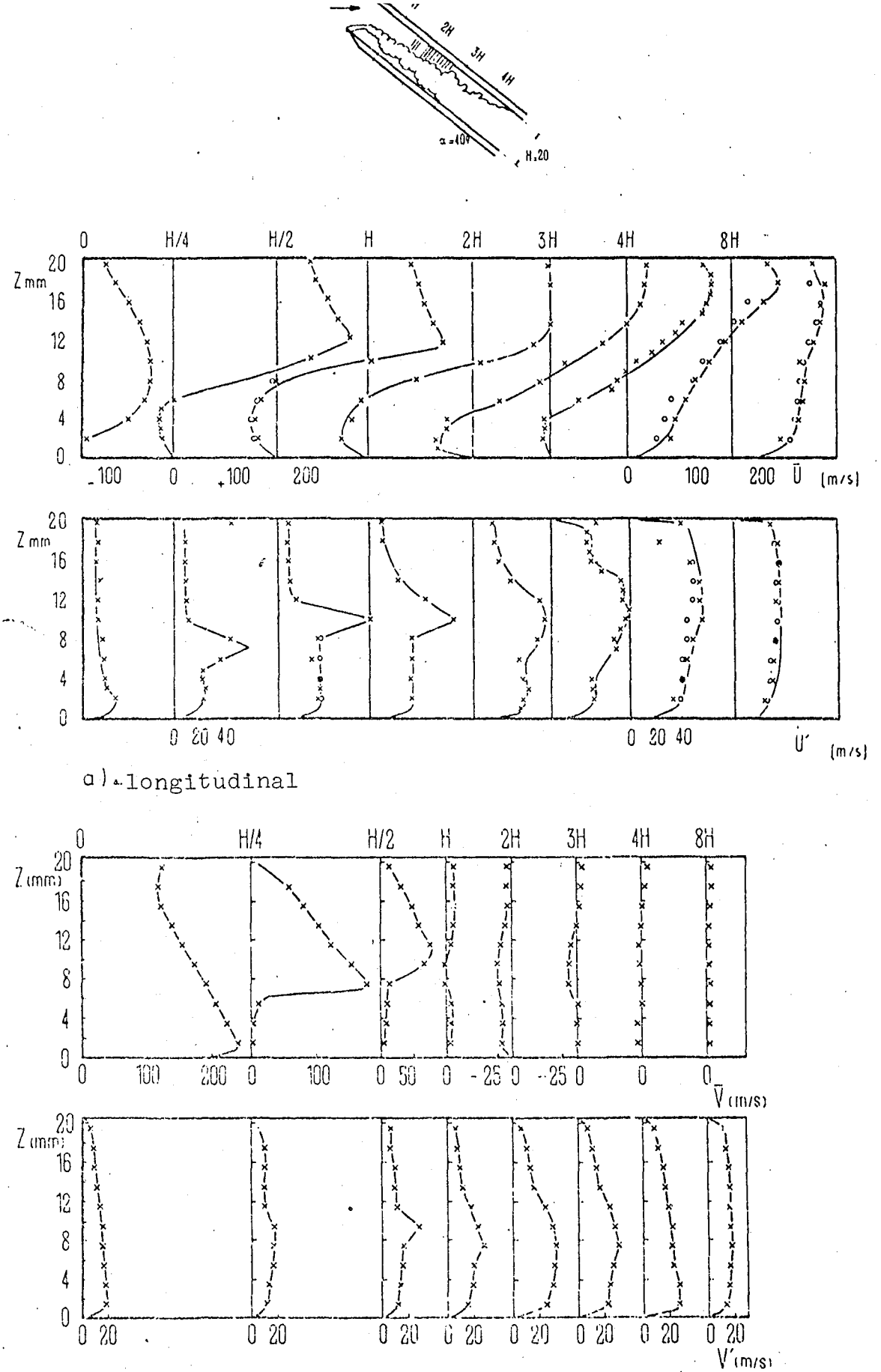

FIGURE 7. MEASUREMENT OF AVERAGE SPEEDS AND FLUCTUATIONS USING LASER ANEMOMETRY

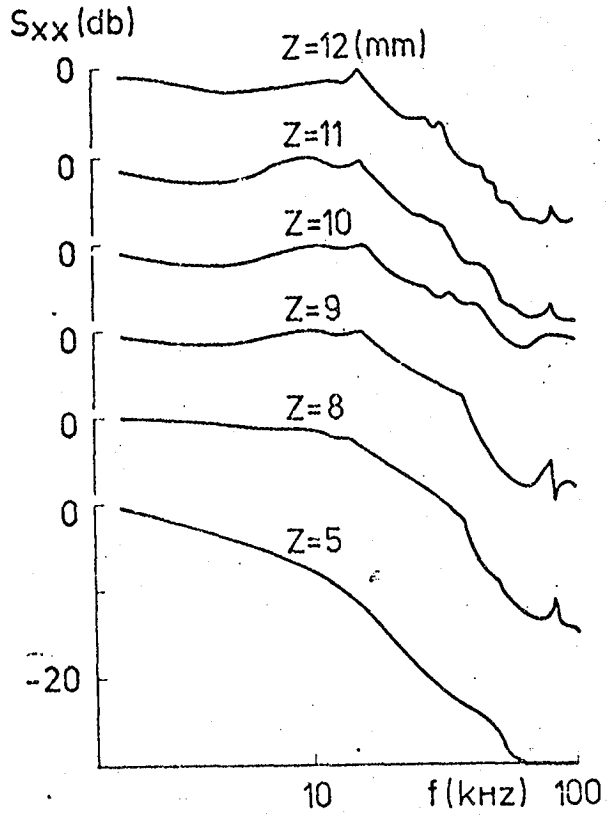

Figure 8a. SPECTRAL ANALYSIS (hot wire)

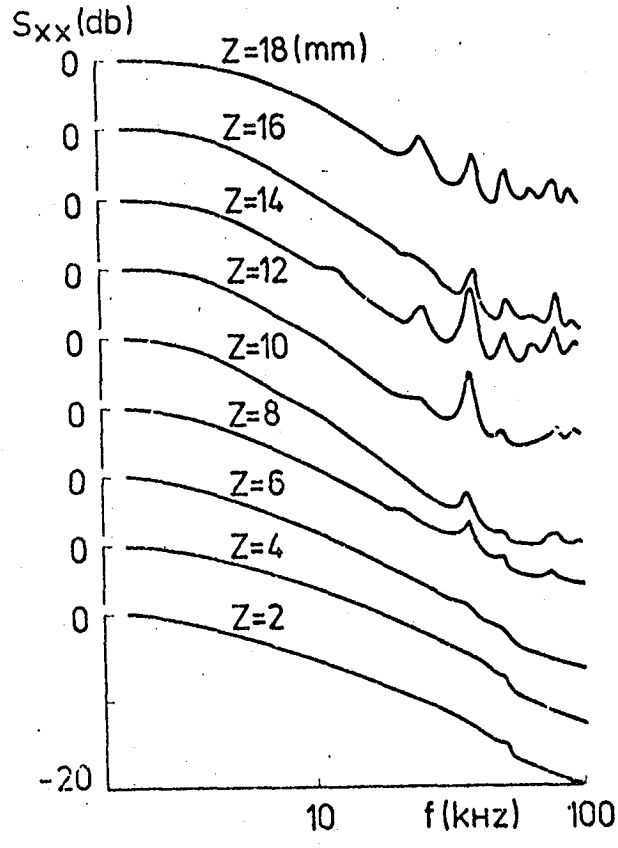

Figure 8b. SPECTRAL ANALYSIS (hot wire)

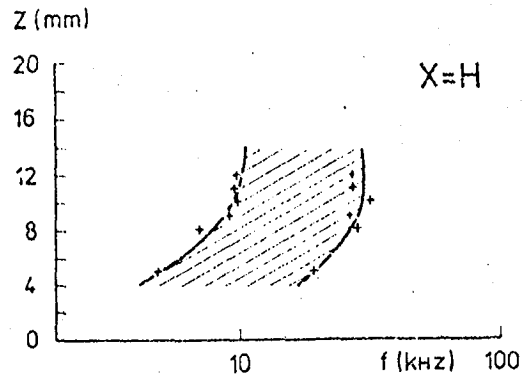

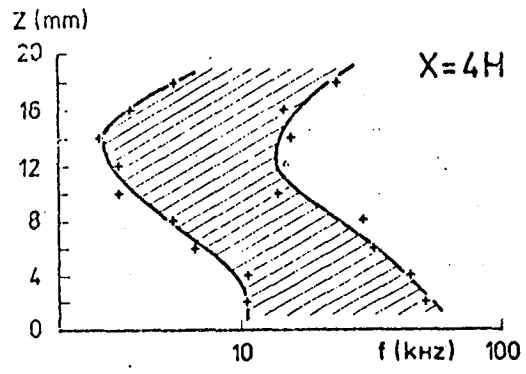

Figure 8c. DISTRIBUTION OF THE MAXIMUM OF SPECTRAL ENERGY